The fully nonlinear stratified geostrophic adjustment problem

A. Coutino and M. Stastna

University of Waterloo, Department of Applied Mathematics, 200 University Ave W, Waterloo, ON N2L 3G1, Canada

Received: 27 November 2015 – Accepted: 1 December 2015 – Published: 18 January 2016

Correspondence to: A. Coutino (acoutino@uwaterloo.ca)

Published by Copernicus Publications on behalf of the European Geosciences Union & the American Geophysical Union.

Abstract

The study of adjustment to equilibrium is a classical problem in geophysical fluid dynamics. We consider the fully nonlinear, stratified adjustment problem from a numerical point of view. We present results of smooth dam break simulations based on experiments in the published literature. We focus on both the wave trains that propagate away from the nascent geostrophic state and the geostrophic state itself. For the Rossby number range considered the rank ordered solitary wave train of the non rotating adjustment problem breaks down into a leading packet-like disturbance and a trailing tail. We consider variations in Rossby number and demonstrate that the wave train emanates from the inertial oscillations of the geostrophic state itself, but that the precise phase of the oscillation that yields the wave train is Rossby number dependent. We quantify the strength of the inertial oscillations of the geostrophic state and find results that are in agreement with hydrostatic theory in the literature. We consider the effects of changes in the polarity of the initial perturbations and find that the leading wave packet never completely separates from the trailing tail in this case. Finally we demonstrate that both polarities yield a unique signature in the spectrum of the depth averaged kinetic energy. This signature is fundamentally different from that found in non-rotating cases, and allows for low rotation rates allows for the discrimination between the polarity of the initial perturbation.

1 Introduction

Geostrophic balance, namely the balance between the pressure gradient and the Coriolis pseudo force, is observed to hold to a good approximation for the large scale motions in the atmosphere and the ocean. The process through which some disturbed state reaches this balance is called geostrophic adjustment. This problem was first considered by Rossby (1937). Using conservation of momentum and mass, he derived the geostrophic steady state corresponding to an initial perturbation. In the original publi-

NPGD

doi:10.5194/npg-2015-73

Fully nonlinear stratified geostrophic adjustment problem

A. Coutino and M. Stastna

cation, Rossby noted that the end state of the system possessed less energy than the initial state. The cause of this difference was identified by Cahn (1945) who showed that the end state is reached via inertial oscillations which disperse energy through waves. Since then, numerous papers have used a variety of methods such as asymptotic expansions and numerical integration to solve this linear problem. There has been a great deal of published work on the linear problem (Ou, 1984; Gill, 1976; Middleton, 1987; Washington, 1964; Mihaljan, 1963), but little on the fully nonlinear one. This is partly because nonlinear problems rarely yield analytical solutions in closed form, and partly because numerical methods applied to the problem must accurately resolve multiple length scales.

Kuo and Polvani (1999), a key paper in the study of the nonlinear problem, considered the adjustment problem in the context of the single layer shallow water equations in one dimension. The authors built on the results of Killworth (1992), and performed a numerical analysis of the fully nonlinear problem with "dam break" initial conditions, see Gill (1982). The authors found that the nonlinearity and rotation led to bore generation, with the bores dissipating energy as they propagated away. Since the nonlinear shallow water equations neglect non-hydrostatic dispersion, these bores manifested as shock-like fronts. This is in contrast to the non rotating stratified adjustment problem which leads to the generation of either a rank ordered train of internal solitary waves, or an undular bore. Indeed, in this dispersive system, for the majority of parameter space, breaking is not observed. The authors also found that the inertial oscillations within the geostrophic state can persist for long times and are highly dependant on the initial conditions.

Rotation influenced nonlinear waves have also been considered using a model nonlinear wave equation; in this case a member of the Korteweg – de Vries (KdV) family of equations. A rotation modified version of the KdV equation was first derived by Ostrovsky (see Grimshaw et al. (2012) for an in-depth discussion of the equation properties and references to the Russian literature). This new equation was subsequently analysed both through theoretical solutions found by asymptotic expansions and through

[NPGD](#)

doi:10.5194/npg-2015-73

Fully nonlinear stratified geostrophic adjustment problem

A. Coutino and M. Stastna

numerical solutions. Investigation of the model equations revealed that the precise balance between nonlinearity and dispersion that leads to the traditional soliton solution of the KdV-equation is destroyed by the addition of rotation, and that over time the soliton breaks down into a nonlinear wave packet, Grimshaw and Helfrich (2008). This hypothesis was later supported by experimental results, Grimshaw et al. (2013). From a theoretical point of view, Grimshaw and Helfrich (2008) also found that the extended Nonlinear Schrodinger (NLS) Equation provides a good qualitative description of the wave packet.

Work has also been performed using models with higher order nonlinearity (Helfrich, 2007) and the full set of stratified Euler equations Stastna et al. (2009). Both of these studies considered the breakdown of an initial solitary wave in the presence of rotation. Helfrich suggested that the initial solitary wave breaks down into a coherent leading wave packet with a trailing tail of waves. Stastna et al. suggested that for large amplitude, exact internal solitary waves that are solutions to the Dubreil–Jacotin–Long (DJL) equation, Helfrich's result was observed for artificially high rotation rates while rotation rates typical of mid-latitudes led to a disturbance that never fully separated from the trailing tail. Stastna et al. also performed collision experiments, finding that the packets that emerge from the initial solitary waves can merge during collisions, and hence do not appear to interact as classical solitons. Stastna et al. also found that by increasing the width of a flat-crested wave, more energy was deposited into the tail. It remains to reconcile the two sets of results, likely by systematically reducing the solitary wave amplitude used as an initial condition.

In this paper we present the results of high resolution simulations of the geostrophic adjustment of a stratified fluid with a single pycnocline on the experimental scale. In the non-rotating situation the initial disturbance develops into a rank-ordered train of solitary waves or an undular bore, depending on the polarity of the initial disturbance. Rotation modifies the situation and the simulations presented below indicate that the initial disturbance evolves into a geostrophic state that remains trapped in the region of the initial disturbance and waves that propagate away. The waves generated disperse

[NPGD](#)

doi:10.5194/npg-2015-73

Fully nonlinear stratified geostrophic adjustment problem

A. Coutino and M. Stastna

into a leading wave packet and trailing wave-train qualitatively in agreement with the predictions of Grimshaw and Helfrich (2008). However, the leading packet cannot be completely separated from the trailing tail on the scale of even the largest experiments.

The geostrophic state oscillates at the inertial frequency, in agreement with the results of Kuo and Polvani (1997). Shock-like bore fronts do not form during the geostrophic adjustment, since the model resolution is sufficient to consider both the large scales influenced by rotation and shorter scales dominated by non hydrostatic effects (despite initial conditions matching breaking cases seen in Kuo and Polvani, 1997).

The Rossby number (Ro) can be varied by modifying either the length scale of the initial disturbance or the rotation rate. Both choices will alter the proportion of energy that remains in the geostrophic state and that propagates away. Moreover, the amplitude of the inertial oscillations that the geostrophic state undergoes will also change. We find qualitatively different behaviour of the leading packet for $Ro = 1.25$ and 0.75. We investigate the effects of polarity of the initial disturbance and find that, as expected, the geostrophic state is unaffected by polarity. We find that at high rotation rates the wave packet behaviour is largely unchanged by changes in polarity. We subsequently investigate the regime of weaker rotation effects. We find that while there is evidence of a wave packet emerging from the undular bore, though the packet never completely separates from the tail, even at higher rotation rates. We illustrate that the spectrum of the vertically averaged kinetic energy is fundamentally different in the rotating case, thereby providing a diagnostic in the rotation modified cases.

2 Methods

For the following numerical simulations, the full set of stratified Euler equations for an incompressible fluid were used, though no span-wise variations were considered. Rotation was incorporated using an f-plane approximation and the non-traditional terms were dropped, see Gerkema et al. (2008) for a review of this process. The

NPGD

doi:10.5194/npg-2015-73

Fully nonlinear stratified geostrophic adjustment problem

A. Coutino and M. Stastna

[NPGD](#)

doi:10.5194/npg-2015-73

Fully nonlinear stratified geostrophic adjustment problem

A. Coutino and M. Stastna

x axis is taken as parallel to the flat ocean bottom with the z axis pointing upward ($\hat{k}$ is the upward directed unit vector). The Euler equations for velocity $\boldsymbol{u} = [u(x,z,t), v(x,z,t), w(x,z,t)]$, density $\rho(x,z,t)$ and pressure $P(x,z,t)$ are,

$$\frac{D\boldsymbol{u}}{Dt} + (-fv, fu, 0) = -\boldsymbol{\nabla}P - \rho' g\hat{k} + \nu\nabla^2\boldsymbol{u}, \tag{1}$$

$$\nabla \cdot \boldsymbol{u} = 0, \tag{2}$$

$$\frac{D\rho}{Dt} = 0. \tag{3}$$

In accordance with convention we have divided the momentum equation by the constant reference density ρ_0 and absorbed the hydrostatic pressure into the pressure P. We make the Boussinesq approximation for density and write $\rho = \rho_0(1 + \overline{\rho}(z) + \rho'(x,z,t))$ where $\overline{\rho}$ is the background density profile and ρ' is considered a small perturbation. Due to our interest in the wave dynamics in the main water column, as opposed to details of the boundary layer dynamics, we impose free slip boundary conditions at the top and bottom of our domain this will also ensure that the boundary layer does not play a significant role in the simulations on which we report. The walls allow us to mimic a lock-release setup that is used to create waves in many laboratory setups (Carr and Davies, 2006; Grue et al., 2000; Helfrich and Melville, 2006). We have elected to neglect the span-wise dimension (y), as the lab results in Grimshaw et al. (2013) were preformed away from any side boundaries and they elected to neglect any curvature from the waves created.

In the following set of experiments the two dimensionless numbers which are dynamically important are the Rossby number and the Reynolds number. The Rossby number is defined as $Ro = \frac{U}{fL}$ where U is the typical wave speed, L is the typical length scale and f is the rotation rate. This reflects a ratio of the inertia term to the Coriolis force term. When the Coriolis force dominates, the fluid can reach a balance between the rotation and pressure terms, i.e., geostrophic balance. The Reynolds number is given as $Re = \frac{UL}{\nu}$, where U and L are the same as for Ro and ν is the kinematic viscosity. In

addition to these traditional dimensionless numbers we also define a nonlinearity parameter α found in Kuo and Polvani (1997), defined as $\alpha = \frac{\eta_0}{H_0}$ where η_0 is the height of the jump in initial conditions and H_0 is the height of the undisturbed fluid column. This parameter can be used to modify the strength of the nonlinearity. The parameter is well suited for shallow water equations. For the full set of Euler equations some ambiguity is introduced by the vertical structure of the stratification and the initial perturbation. Nevertheless we have found α to be a useful parameter, likely since the disturbances in our simulations are dominated by mode-1 waves.

The numerical simulations presented here were preformed using an incompressible Navier Stokes equation solver which implements a pseudo-spectral collocation method (SPINS), presented in Subich et al. (2013). The solver uses spectral methods resulting in the accuracy scaling with the number of grid points. To deal with the build up of energy in the high wave numbers an exponential filter is used after a specific wave number cut off (for details of the model see Subich et al., 2013).

We performed a series of 2-D lab scale numerical simulations on a similar scale to the physical experiments seen in Grimshaw and Helfrich (2008) which were preformed using the 13 m diameter rotating platform at the LEGI-Coriolis Laboratory in Grenoble. Motivated by the results presented in Stastna et al. (2009), we elected to use a domain four times larger than the physical tank, as the 13 m is an insufficient length when considering lower (closer to physical) rotation rates. In addition to this it was decided to change the tank depth to a more evenly divisible 40 cm (from their 36 cm). The density difference was set at 1 %. 8192 grid points were used to resolve the 52 m length of the tank and 192 points were used for the 40 cm height, providing a 6 mm horizontal resolution and 2 mm vertical resolution. To easily compare these numerical results to the experimental ones in Grimshaw et al. our rotation rate was based on their lowest presented f which had a value of $0.105\,\mathrm{s}^{-1}$. It was also decided to base the initial perturbation width w_0 on twice the Rossby radius of deformation so as to allow for a neater examination of the parameter space. In each of the simulations that were run the initial conditions were given by a quiescent fluid, and a density field defined via the

Discussion Paper | Discussion Paper | Discussion Paper | Discussion Paper |

[NPGD](#)

doi:10.5194/npg-2015-73

Fully nonlinear stratified geostrophic adjustment problem

A. Coutino and M. Stastna

[NPGD](#)

doi:10.5194/npg-2015-73

Fully nonlinear stratified geostrophic adjustment problem

A. Coutino and M. Stastna

isopycnal displacement η.

$$\rho(x, z, t = 0) = \overline{\rho}(x, z - \eta) = 0.005 \tanh\left(\frac{z - 0.3 - \eta}{0.01}\right),$$

$$\eta = \pm 0.05 \exp\left[-\left(\frac{x}{w}\right)^8\right],$$

where w is the half width of the initial perturbation and the sign changes correspond to changes in jump orientation.

3   Results

In this section we present the results of multiple numerical simulations. The primary way in which the parameters were modified was by changing either the initial width of the perturbation or by changing the rotation rate. Using the initial width as the typical length scale, $L = w$, we are thus varying the Rossby number. The resulting values of the dimensionless parameter are shown in Table 1. Across all the cases, the depth does not change, and hence neither does the two-layer linear long wave speed $U = \sqrt{g\frac{\Delta\rho}{\rho_0}\frac{H_1 H_2}{H_1 + H_2}} = 0.0858 \, \mathrm{m \, s^{-1}}$ where $g = 9.81 \, \mathrm{m \, s^{-2}}$, $\Delta\rho = 0.01$, $\rho_0 = 1$, $H_1 = 0.3 \, \mathrm{m}$ and $H_2 = 0.1 \, \mathrm{m}$; this implies that there are two readily accessible ways to create a situation with the same Rossby number. Using the same wave speed and length scales as for the Rossby number, the corresponding Reynolds numbers are presented in Table 2; the kinematic viscosity was the same for all simulations, $v = 1e^{-6} \, \mathrm{m^2 \, s^{-1}}$. It is also possible to define a Reynolds number based on the channel depth, $L = 0.4 \, \mathrm{m}$, providing a corresponding $Re = 3.43 \times 10^5$; this would be the same for all cases since domain depth does not change. Several additional experiments were carried out changing the initial wave amplitude which results in different "nonlinearity" parameters. For the initial amplitude of $\eta_0 = 0.05 \, \mathrm{m}$ and $H_0 = 0.3 \, \mathrm{m}$ we have $\alpha = 0.1667$. For the cases where amplitude is halved and quartered corresponding alpha values are $\alpha = 0.0833$ and 0.0416.

Discussion Paper | Discussion Paper | Discussion Paper | Discussion Paper

The initial value of $\alpha = 0.1667$ allows for an easy comparison to many of the figures in Kuo and Polvani (1997) which are based on a value of 0.1.

In addition to the simulations above, another set of simulations were performed using the opposite polarity of the initial disturbance. These opposite polarity simulations correspond exactly to the cases seen in Table 1 the only difference being the sign in the isopycnal displacement used in the initial conditions.

Several simulations were also preformed on an extra-long tank to investigate the long-time results of adjustment. For these simulations the tank length was $L = 260\,\text{m}$ and the number of horizontal grid points was increased to 16 384, providing a 1.58 cm resolution. The vertical hight and grid points were kept the same from the smaller case.

Unless otherwise stated the following scaling is used for all figures: $T = 1/f$, $L_z = Lz$ and $L_x = Ro_r$ where $Ro_r = \frac{U}{f}$ is the Rossby radius of deformation and $Lz = 0.4\,\text{m}$ is the depth of the tank. For kinetic energy, we scale by the maximum kinetic energy. For the convenience of experimentalists, we report both physical and dimensionless time in the figure captions.

3.1 Non-rotating cases

We begin by reproducing the results for the adjustment problem without rotation. The solution to this problem is well known, and yields either a rank ordered train of solitary waves, or an undular bore forming from the initial disturbance, depending upon the polarity of the initial disturbance. The two cases are shown in Fig. 1. Since there is no rotation, the advective time-scale was chosen to nondimensionalize time, $T = L/U$ (the initial width $w = \frac{1}{2}w_0$ was chosen for the typical length-scale). The stark difference between these cases is readily apparent in both types of plots. The solutions to this problem have already been extensively investigated, and as such we will forgo a detailed discussion here however this behaviour will be used to compare later results.

[NPGD](#)

doi:10.5194/npg-2015-73

Fully nonlinear stratified geostrophic adjustment problem

A. Coutino and M. Stastna

Discussion Paper | Discussion Paper | Discussion Paper | Discussion Paper

3.2 General evolution

Comparing the value of our Rossby numbers to those discussed in Grimshaw et al., we find that their case with a rotation rate of $0.105\,\text{s}^{-1}$ had a corresponding Rossby number of 0.667; thus, we use the $f = f_0$ and $w = w_0$ case as our baseline as it has $Ro = 0.5$ which is in the same regime as their number. Snapshots of the time evolution for this case are provided in Fig. 2.

Observing the structure that appears throughout the time series, we argue that these waves closely resemble a modulated wave packet as presented in Grimshaw et al. (1998) instead of the rotation modified bore seen in Kuo and Polvani (1997). When comparing to the work done by Kuo and Polvani we first note that for our simulations the nonlinear parameter is quite small at $\alpha \approx 0.166$, however their work suggests that even for this small value and smooth initial condition breaking will still occur. The present simulations were carried out with the full set of Euler equations. As such the dispersion that is neglected in the shallow water equations used by Kuo and Polvani becomes important when the wave front steepens. Dispersion breaks the front down into a train of smaller waves and eliminates shock formation. In addition to the change in steepening dynamics, the initially tightly packed waves disperse over time, yet are observed to remain bound together. For this reason we find that the modulated wave packet is a better description for these dynamics.

While the base case of Fig. 2 allows us to easily compare with the results from the LEGI-Coriolis tank with its relatively high rotation rate, in order to compare to what is observable in coastal waters or large lakes, we must consider lower rotation rates. While still being constrained by the size of our extended tank, it was decided to focus on a half and a quarter of the original rotation rate. Figure 3 shows space–time plots of the vertically integrated kinetic energy for these three rotation rates, with the initial width held the same at $w = w_0$. Figure 3a corresponds to case the base case in Fig. 2, while Fig. 3b to $f = \frac{1}{2}f_0$, and Fig. 3c to $f = \frac{1}{4}f_0$. Comparing to Table 1 we see that these cases have $Ro = \frac{1}{2}$, $Ro = 1$ and $Ro = 2$ respectively. In all cases, we can easily identify

NPGD

doi:10.5194/npg-2015-73

Fully nonlinear stratified geostrophic adjustment problem

A. Coutino and M. Stastna

the geostrophic state that forms from the initialization near the left hand boundary of the model tank and observe that it oscillates, or pulsates, in time. This is in qualitative agreement with the results from Kuo and Polvani. These pulses are particularly evident in Fig. 3a and b. Comparing the three plots we see that with the decrease in rotation rate we shift the location where, and the time when, the most energetic waves are ejected from the pulsating, geostrophic region. In Fig. 3c the kinetic energy is ejected almost immediately, and by the time the second pulse is visible in the geostrophic region the wave packet is well away from the left boundary. As the wave propagates away, it develops a clear wave packet structure which can be easily identified in the space–time plots. In Fig. 3b we see that the strongest kinetic energy propagates away from the second half of the initial pulse, but also develops a packet structure as it moves away from the geostrophic region. Differences arise when we look at Fig. 3a, which has the highest rotation rate, where a small packet is generated however it is forms from the second pulse. Key to note for this case is that by $t = 286\,\text{s}$ (30) the kinetic energy stops reaching a significant level within the packet. As expected, reducing the rotation rate leads to a weaker geostrophic state and more energy in the initial pulse of kinetic energy. Also note that from Fig. 3a and b there is evidence of waves being continuously ejected from the geostrophic state, even for late times in the simulation.

3.3 Geostrophic state

In the rotation modified adjustment problem there are two dominant features, the geostrophic state that is leftover from the initial conditions and the train of Poincaré waves which carries energy away from it. For this section we will focus on the dynamics, and changes, of the geostrophic state.

Figure 4 shows space–time plots of vertically integrated kinetic energy for five cases of different initial widths where the rotation rate has been held constant at $f = f_0$. These cases have Rossby numbers 2, 1, $\frac{1}{2}$, $\frac{1}{4}$ and $\frac{1}{8}$ for Fig. 4a–e respectively. This figure extends the trend seen in Fig. 3 where in this case increasing the initial width modifies the temporal phase of the geostrophic state's oscillation that leads the wave packet

[NPGD](#)

doi:10.5194/npg-2015-73

Fully nonlinear stratified geostrophic adjustment problem

A. Coutino and M. Stastna

Discussion Paper | Discussion Paper | Discussion Paper | Discussion Paper |

generation. In particular, the generation occurs during the onset of the first pulse in Fig. 4a and shifts to the middle of the fourth pulse in Fig. 4e. We can also note from this figure that as the initial width is increased, more energy is trapped in the geostrophic state, so that in Fig. 4e almost no energy is ejected via the packet. To further investigate the geostrophic state (shown as the blue dashed line in Fig. 4), the vertically integrated kinetic energy was extracted from this point and is shown separately in Fig. 5a with different colours corresponding to the different cases. It is important to remember that the rotation rate is constant for all of these cases and so inertial oscillations should have the same period. From the plots, we see that the first oscillation appears in roughly the same place for all the cases, but after that there appears to be some phase shifting. However, the $\frac{1}{2}w_0$ and $\frac{1}{4}w_0$ cases are always in phase. Other than the $w = 2w_0$ and $w = 4w_0$ case, the rest of the cases eventually reach a stationary state (or in other words oscillations are too small to be seen on the scale of the graph). The $2w_0$ case looks as if it is in the process of reaching its stationary state, but the $4w_0$ case looks as if the oscillations have reached a constant size and do not seem to decrease. From these results the conclusion is that the $w = w_0$ case appears to settle into the most energetic stationary state. Figure 5b shows the spectral power of the respective time series which clearly shows that all the cases have a strong spike in power around the inertial frequency confirming the results from Kuo and Polvani (1997).

We next consider the time evolution of the proportion of total kinetic energy inside of the geostrophic state to that outside, this is shown in Fig. 6. In this figure we have the same cases as in Fig. 5, $f = f_0$, but separated into their own plots (the panels descend from smallest initial width, $w = \frac{1}{4}w_0$ in Fig. 6a to largest, $w = 4w_0$ in Fig. 6e). The red line is the energy outside the geostrophic state while blue corresponds to that inside. Some immediate features are apparent from the figure: for small initial width, Fig. 6a there is more energy outside of the geostrophic state starting from an early time. The opposite is true for the large case, Fig. 6e, where all the energy is located inside the state and very little outside. In the three intermediate cases we see that there is roughly

Discussion Paper | Discussion Paper | Discussion Paper | Discussion Paper |

[NPGD](#)

doi:10.5194/npg-2015-73

Fully nonlinear stratified geostrophic adjustment problem

A. Coutino and M. Stastna

a balance between the energy inside and outside the state, though the point where they are equal occurs later as we increase the width.

3.4 Rossby number variation

The cases where the rotation rate or initial width was varied, can be interpreted as changing the Rossby number. With this in mind we investigate the results of keeping the Rossby number constant across changes in rotation by making a corresponding change in the initial width.

Figure 7 shows the space–time plots of kinetic energy for the same Rossby number formed using different combinations of rotation rate and initial width. The top three panels show the full evolution of the cases while the bottom three show a scaled version of the panel above. We have calculated the vertically integrated kinetic energy across the entire domain. The most striking feature of the top three panels in the figure is that dynamically they look the same, we have a primary, energetic wave packet produced from the first pulse of the geostrophic state, and this packet propagates away without very much spreading. We can also see that the oscillations of the geostrophic state remain quite evident for later times. The bottom three panels show rescaled plots and the similarities between the cases are immediately visible. The geostrophic state looks almost identical between the three cases; the inertial oscillations occur at nearly the same location in scaled space and have nearly the same intensity. While looking roughly similar, some differences arise in the wave-train that is ejected, specifically we can see that the number and duration of the peaks of the wave-train are different across the three cases; especially between Fig. 7d and e.

Based on these similarities and the differences from Fig. 3 we wanted to investigate the transition region around the critical Rossby number, $Ro = 1$, and how the dynamics change depending on the value ($Ro > 1$ corresponding to stronger inertia, while $Ro < 1$ to a stronger Coriolis force). Figure 8a corresponds to $Ro = 1.25$ and Fig. 8b to $Ro = 0.75$, for both of these simulations, width was varied to change the Rossby number and f was set to f_0. There are several features which are immediately obvious: first is the

Discussion Paper | Discussion Paper | Discussion Paper | Discussion Paper |

[NPGD](#)

doi:10.5194/npg-2015-73

Fully nonlinear stratified geostrophic adjustment problem

A. Coutino and M. Stastna

shift in phase of the ejected wave packet. The packet is ejected from the front of the first pulse in the $Ro = 1.25$ case while in the $Ro = 0.75$ case the packet originates at the back of the first pulse (almost at the front of the second pulse), this was also seen in Fig. 3 when rotation rate was changed. The second feature is that the geostrophic state is significantly wider and stronger in the $Ro = 0.75$ case. This is consistent with the idea that the Coriolis force is stronger and can trap more energy in the geostrophic state. The last feature worth noting is that in the $Ro = 0.75$ case, there is much more spreading of the wave packet as it travels through the tank. The results from this figure support the evidence seen in Fig. 4 where crossing from below to above one Rossby number corresponds to a change in the dynamics.

3.5 Polarity effects

From the standard KdV theory there is a qualitative difference in the types of waves that are generated from an initial disturbance with negative polarity (a wave of depression) compared to one with a positive polarity (a wave of elevation). In particular, disturbances with negative polarity will yield a rank ordered solitary wave train while those with a positive polarity will yield an undular bore. To investigate this effect for this more general rotation modified adjustment problem we simulated all of the cases from Table 1 a second time with the polarity of the initial conditions reversed.

Figure 9 provides an outline of the time evolution of density for two cases, where their initial polarity is the is the only difference. The base case of $w = w_0$ and $f = f_0$ is shown. The left column corresponds to starting with an initial wave of depression, while the right column corresponds to an initial wave of elevation. Figure 9a and b are taken at $t = 75\,\mathrm{s}$ (5.25), Fig. 9c and d at $t = 300\,\mathrm{s}$ (21) and Fig. 9e and f at $t = 525\,\mathrm{s}$ (36.75). From these snapshots the only difference that appears to occur is that the waves created are of the opposite polarity, and other than this the two packets look almost identical. More differences are apparent from the space–time plot in Fig. 10 which shows the vertically integrated kinetic energy; from these plots we can see that the positive polarity case Fig. 10b contains more kinetic energy in both the geostrophic

Discussion Paper | Discussion Paper | Discussion Paper | Discussion Paper | Discussion Paper |

[NPGD](#)

doi:10.5194/npg-2015-73

Fully nonlinear stratified geostrophic adjustment problem

A. Coutino and M. Stastna

state and in the wave packet. Dynamically, however, the two cases look almost identical with packet ejection and dispersion occurring at the same times and places but the positive polarity cases appears to have higher kinetic energies at all times. This result is fundamentally different from theory based on KdV which predicts qualitatively different results based on polarity.

Starting from our base case with $w = w_0$ and $f = f_0$, we also ran a series of cases with a reduced amplitude of the initial perturbation. From the cases that were run there was no discernible difference to any of the fields within the waves generated once they had been scaled by the factor that the amplitude was reduced. The only difference that appeared was the shape of the geostrophic state, with the large amplitude cases retaining a larger hump. However the maximum v, or span-wise velocity within the state, scales with the amplitude. It is possible that were we to allow for spawns variation the stronger geostrophic states could undergo a spawns instability, though this remains a topic for future investigation.

Due to the presence of the leading wave train in the density contours it was decided to investigate whether the leading packet would separate from the wave tail as Grimshaw et al. argue or whether it remains locked to the tail as Stastna et al. found. We also wished to contrast the behaviour for situations in which a significant portion of energy was deposited into the wave train (low rotation rate) and those in which the geostrophic state was dominant (high rotation rate).

Figure 11 shows the density contours for a positive polarity case with initial width $w = \frac{1}{2}w_0$ and rotation rate $f = \frac{1}{8}f_0$. For this case the length of the tank was increased by five times to a total length of 260 m, the horizontal resolution was doubled to 16 384 points which provides 1.59 cm resolution for this case. For this lower rotation rate the first two panels, Fig. 11a and b, look very similar to the non-rotating positive case of an undular bore. However for later times, the last two panels (Fig. 11c and d), it is possible to identify packet like features at the front of the "bore", this is especially true in the final figure. Despite the large length and temporal scales it does not appear that this packet separates from the wave-train in agreement with Stastna et al. (2009). Further

NPGD

doi:10.5194/npg-2015-73

Fully nonlinear stratified geostrophic adjustment problem

A. Coutino and M. Stastna

Discussion Paper | Discussion Paper | Discussion Paper | Discussion Paper

simulations were run with rotation rate being $f = \frac{1}{2}f_0$ and $f = 2f_0$ with the same initial width to see whether by increasing rotation, thus reducing Rossby number, we could get separation. However in both of these cases the packet again failed to separate from the tail, though the packet became much more dominant compared to the tail.

The long-time simulations were also used to compare the differences in the geostrophic state between the positive and negative polarity cases, the results of this analysis is presented in Fig. 12. For these cases the rotation rate was set to $f = 2f_0$ and the initial width was $w = \frac{1}{2}w_0$ resulting in a Rossby number of $\frac{1}{2}$. Figure 12a clearly shows the energy difference that was mentioned in the discussion of Fig. 10, indicating that the positive polarity case appears more efficient at keeping energy in the geostrophic state. Figure 12b shows the logarithm time series of kinetic energy after the packet has been ejected. If we ignore the inertial oscillations (which appear to be rapid on the time scale shown) we can see a clear decay. By computing the logarithm of the time series (Fig. 12b) we are able to show that the decay is nearly exponential, with the positive polarity case decaying roughly 5 % faster. The decay rate decreases with increasing time. The bottom two panels, Fig. 12c and d, show the kinetic energy (scaled by its maximum) in the geostrophic state along with three superimposed lines of constant density. It is clear that the polarity of the geostrophic state strongly modifies the distribution of the kinetic energy, and indeed that the positive polarity case is strongly affected by the boundaries.

When we look at the density contours of the wave-train, shown in Fig. 13, we see that there are substantial differences between the polarities in the low ($f = \frac{1}{8}f_0$) rotation case, Fig. 13a and b. Despite having rotation, we see a result that at least bears some resemblance to the non-rotating case. This changes substantially when we consider the high ($f = 2f_0$) rotation case Fig. 13c and d. In these cases the waves are almost indistinguishable from each other. An important difference to notice between the high and low rotation cases is that the amplitude of the ejected waves is significantly reduced. We argue that this collapse of the different polarities into the same dynamics for higher

Discussion Paper | Discussion Paper | Discussion Paper | Discussion Paper | Discussion Paper |

[NPGD](#)

doi:10.5194/npg-2015-73

Fully nonlinear stratified geostrophic adjustment problem

A. Coutino and M. Stastna

Title Page

Abstract | Introduction

Conclusions | References

Tables | Figures

|◄ | ►|

◄ | ►

Back | Close

Full Screen / Esc

rotation rates is a result of the geostrophic state capturing more energy, resulting in smaller amplitude waves being ejected and thus decreasing the effect of nonlinearity.

A natural question to ask is whether the effects of rotation are clearly reflected in the spectrum of the waves, particularly for the lower rotation rates. Figure 14 shows the spectra of the two polarity cases for two different rotation rates, one low ($f = \frac{1}{8}f_0$), Fig. 14a, and one high ($f = 2f_0$), Fig. 14b; they correspond to Rossby numbers $Ro = 8$ and $Ro = \frac{1}{2}$ respectively. It should be clear from Fig. 14a that in this low rotation case the spectra are not entirely similar. While the positive polarity case matches the first spike in wave-number at ≈ 10 the negative case quickly drops off in power, while the positive cases exhibits several spikes at smaller values of the wave-number. The picture changes dramatically in the high case. In this case, other than a slight phase shift, the spectra are almost identical. The spikes in spectra occur at the same wave-number and are of the same order. This result provides further evidence supporting the claim we have made previously that as we increase the rotation rate, starting from two different polarities, the dynamics collapse to a common result.

To investigate the transition from distinct to uniform dynamics, we examined at the differences in spectra of the ejected waves for the low rotation rate from the previous figure and the case of no rotation. This is presented in Fig. 15. Figure 15a corresponds an initial wave of elevation while Fig. 15b to one of depression. In the case of initial elevation, we can see that when rotation is introduced we increase the power at specific wave-numbers. A similar observation can be made based on panel Fig. 15b, in which the Gaussian-like profile typical of a solitary wave is destroyed by rotation, in favour of peaks at specific wave-numbers. These results suggest that a spectral analysis will reveal the results of rotation equally well for both polarities. This is important since the solitary wave case (in the absence of rotation) can be described quite succinctly, but the unduly bore spreads spatially with increasing time.

[NPGD](http://dx.doi.org/10.5194/npg-2015-73)

doi:10.5194/npg-2015-73

Fully nonlinear stratified geostrophic adjustment problem

A. Coutino and M. Stastna

Discussion Paper | Discussion Paper | Discussion Paper | Discussion Paper

4 Conclusions

In this paper we have taken a systematic approach to the classical rotation-modified stratified adjustment problem. In contrast to what was presented in Kuo and Polvani (1997) we have shown that by using the fully nonlinear Euler equations the waves that are ejected from the geostrophic state do not steepen to a shock. By mapping out the parameter space we have shown that, as expected, the Rossby number is the controlling variable for the dynamics in this problem; when the Rossby number is above one we have that a wave packet is ejected from the first inertial wave pulse of the geostrophic state and does not disperse much as it propagates through the tank. In the cases when Rossby number is less than one, the packet is ejected from a later pulse (smaller Rossby numbers corresponding to later pulses) and disperses as it moves through the tank. We characterized the similarities and differences in the dynamics for cases when the same Rossby number is achieved by different means. We found that for the same Rossby number the dynamics of the geostrophic state are nearly identical, and there are some small differences between the wave-trains but the dynamics are very similar. Our results also show that the oscillations in the geostrophic state are indeed inertial oscillations and can persist for long times, in agreement with Kuo and Polvani (1997). It was also found that in cases with $Ro \leq \frac{1}{8}$ almost all the energy in the system was trapped within the geostrophic state. In contrast with the non-rotating case, differences in initial wave polarity did not lead to different types of waves, and in both positive and negative polarity cases the dynamics of the wave train were practically identical. We argue that the increase in rotation rate traps more energy in the geostrophic state and as a result the waves ejected are smaller in amplitude. As a result of this reduction in amplitude the dynamics are linear and thus the nonlinear polarity differences disappear. The geostrophic state in these cases exhibits a large isopycnal deflection and thus reflects polarity differences. By extending the spatial extent of our simulation and letting our system evolve for a longer time we have shown that the wave-packet, at the front of the wave-train that is created, does not separate from the tail.

Discussion Paper | Discussion Paper | Discussion Paper | Discussion Paper |

NPGD

doi:10.5194/npg-2015-73

Fully nonlinear stratified geostrophic adjustment problem

A. Coutino and M. Stastna

Finally, we used lower rotation rates to demonstrate that the rotation modified dynamics can be successfully detected in the spectrum of the vertically averaged kinetic energy. We also used the spectrum of the wave-packets to explore the way that the polarity differences in the non-rotating case collapse when rotation is introduced.

Future work should consider span-wise variations, especially in the case of the strong geostrophic state for which novel instabilities may be possible. Systematic studies of the shoaling of rotation modified solitary waves and undular bores should also be carried out, since it is not known in what manner these may be different from shoaling in the non rotating case.

This research was supported by the Natural Sciences and Engineering Research Council of Canada.

References

Cahn, A.: An investigation of the free oscillations of a simple current system, J. Meteorol., 2, 113–119, doi:10.1175/1520-0469(1945)002<0113:AIOTFO>2.0.CO;2, 1945. 3

Carr, M. and Davies, P. A.: The motion of an internal solitary wave of depression over a fixed bottom boundary in a shallow, two-layer fluid, Phys. Fluid., 18, 016601, doi:10.1063/1.2162033, 2006. 6

Gerkema, T., Zimmerman, J. T. F., Maas, L. R. M., and van Haren, H.: Geophysical and astrophysical fluid dynamics beyond the traditional approximation, Rev. Geophys., 46, RG2004, doi:10.1029/2006RG000220, 2008. 5

Gill, A.: Atmosphere–Ocean Dynamics, Academic Press, San Diego, USA, available at: https://books.google.ca/books?hl=en&lr=&id=8kFPh_SvnAIC&oi=fnd&pg=PP1&dq=Atmosphere+Ocean+dynamics+Gill&ots=B82Q2v1Umm&sig=eN5ANYnstDvva2w2fLdWLKGHgaA (last access: 21 December 2015), 1982. 3

Gill, A. E.: Adjustment under gravity in a rotating channel, J. Fluid Mech., 77, 603–621, doi:10.1017/S0022112076002280, 1976. 3

Grimshaw, R. and Helfrich, K.: Longtime solutions of the ostrovsky equation, Stud. Appl. Math., 121, 71–88, available at: http://onlinelibrary.wiley.com/doi/10.1111/j.1467-9590.2008.00412.x/full (last access: 21 December 2015),, 2008. 4, 5, 7

[NPGD]

doi:10.5194/npg-2015-73

Fully nonlinear stratified geostrophic adjustment problem

A. Coutino and M. Stastna

Discussion Paper | Discussion Paper | Discussion Paper | Discussion Paper

Grimshaw, R. H. J., Ostrovsky, L. A., Shrira, V. I., and Stepanyants, Y. A.: Long nonlinear surface and internal gravity waves in a rotating ocean, Surv. Geophys., 19, 289–338, doi:10.1023/A:1006587919935, 1998. 10

Grimshaw, R. H. J., Helfrich, K., and Johnson, E. R.: The reduced Ostrovsky equation: integrability and breaking, Stud. Appl. Math., 129, 414–436, doi:10.1111/j.1467-9590.2012.00560.x, 2012. 3

Grimshaw, R. H. J., Helfrich, K. R., and Johnson, E. R.: Experimental study of the effect of rotation on nonlinear internal waves, Phys. Fluids, 25, 056602, doi:10.1063/1.4805092, 2013. 4, 6, 7, 10, 15

Grue, J., Jensen, A., Rusås, P.-O., and Sveen, J. K.: Breaking and broadening of internal solitary waves, J. Fluid Mech., 413, 181–217, doi:10.1017/S0022112000008648, 2000. 6

Helfrich, K. R.: Decay and return of internal solitary waves with rotation, Phys. Fluids, 19, 026601, doi:10.1063/1.2472509, 2007. 4

Helfrich, K. R. and Melville, W. K.: Long nonlinear internal waves, Annu. Rev. Fluid Mech., 38, 395–425, doi:10.1146/annurev.fluid.38.050304.092129, 2006. 6

Killworth, P. D.: The time-dependent collapse of a rotating fluid cylinder, J. Phys. Oceanogr., 22, 390–397, doi:10.1175/1520-0485(1992)022<0390:TTDCOA>2.0.CO;2, 1992. 3

Kuo, A. and Polvani, L.: Time-dependent fully nonlinear geostrophic adjustment, J. Phys. Oceanogr., 27, 1614–1634, doi:10.1175/1520-0485(1997)027<1614:TDFNGA>2.0.CO;2, 1997. 5, 7, 10, 11, 12, 18

Kuo, A. C. and Polvani, L. M.: Wave–vortex interaction in rotating shallow water. Part 1. One space dimension, J. Fluid Mech., 394, 1–27, 1999. 3

Middleton, J. F.: Energetics of linear geostrophic adjustment, J. Phys. Oceanogr., 17, 735–740, doi:10.1175/1520-0485(1987)017<0735:EOLGA>2.0.CO;2, 1987. 3

Mihaljan, J.: The exact solution of the Rossby adjustment problem, Tellus A, 15, 150–154, doi:10.1111/j.2153-3490.1963.tb01373.x, 1963. 3

Ou, H. W.: Geostrophic adjustment: a mechanism for frontogenesis, J. Phys. Oceanogr., 14, 994–1000, doi:10.1175/1520-0485(1984)014<0994:GAAMFF>2.0.CO;2, 1984. 3

Rossby, C.: On the mutual adjustment of pressure and velocity distributions in certain simple current systems, J. Mar . Res., 1, 239–263, available at: http://www.aos.princeton.edu/WWWPUBLIC/gkv/history/Rossby-adj38.pdf (last access: 21 December 2015), 1937. 2

NPGD

doi:10.5194/npg-2015-73

Fully nonlinear stratified geostrophic adjustment problem

A. Coutino and M. Stastna

Stastna, M., Poulin, F. J., Rowe, K. L., and Subich, C.: On fully nonlinear, vertically trapped wave packets in a stratified fluid on the f-plane, Phys. Fluids, 21, 106604, doi:10.1063/1.3253400, 2009. 4, 7, 15

Subich, C. J., Lamb, K. G., and Stastna, M.: Simulation of the Navier–Stokes equations in three dimensions with a spectral collocation method, Int. J. Numer. Meth. Fl., 73, 103–129, doi:10.1002/fld.3788, 2013. 7

Washington, W. M.: A note on the adjustment towards geostrophic equilibrium in a simple fluid system, Tellus, 16, 530–534, doi:10.1111/j.2153-3490.1964.tb00189.x, 1964. 3

NPGD

doi:10.5194/npg-2015-73

Fully nonlinear stratified geostrophic adjustment problem

A. Coutino and M. Stastna

NPGD

doi:10.5194/npg-2015-73

Fully nonlinear stratified geostrophic adjustment problem

A. Coutino and M. Stastna

Table 1. Rossby number of each simulation, where $f_0 = 0.105\,\mathrm{s}^{-1}$ and $w_0 = 1.63\,\mathrm{m}$.

Ro	$\frac{1}{4}w_0$	$\frac{1}{2}w_0$	w_0	$2w_0$	$4w_0$
f_0	2	1	$\frac{1}{2}$	$\frac{1}{4}$	$\frac{1}{8}$
$\frac{1}{2}f_0$	4	2	1	$\frac{1}{2}$	$\frac{1}{4}$
$\frac{1}{4}f_0$	8	4	2	1	$\frac{1}{2}$

NPGD

doi:10.5194/npg-2015-73

Fully nonlinear stratified geostrophic adjustment problem

A. Coutino and M. Stastna

Table 2. Reynolds number of each simulation, where $f_0 = 0.105\,\text{s}^{-1}$ and $w_0 = 1.63\,\text{m}$.

Re	$\frac{1}{4}w_0$	$\frac{1}{2}w_0$	w_0	$2w_0$	$4w_0$
f_0	3.495×10^4	6.990×10^4	1.398×10^5	2.796×10^5	5.593×10^5
$\frac{1}{2}f_0$	3.495×10^4	6.990×10^4	1.398×10^5	2.796×10^5	5.593×10^5
$\frac{1}{4}f_0$	3.495×10^4	6.990×10^4	1.398×10^5	2.796×10^5	5.593×10^5

Discussion Paper | Discussion Paper | Discussion Paper | Discussion Paper

NPGD

doi:10.5194/npg-2015-73

Fully nonlinear stratified geostrophic adjustment problem

A. Coutino and M. Stastna
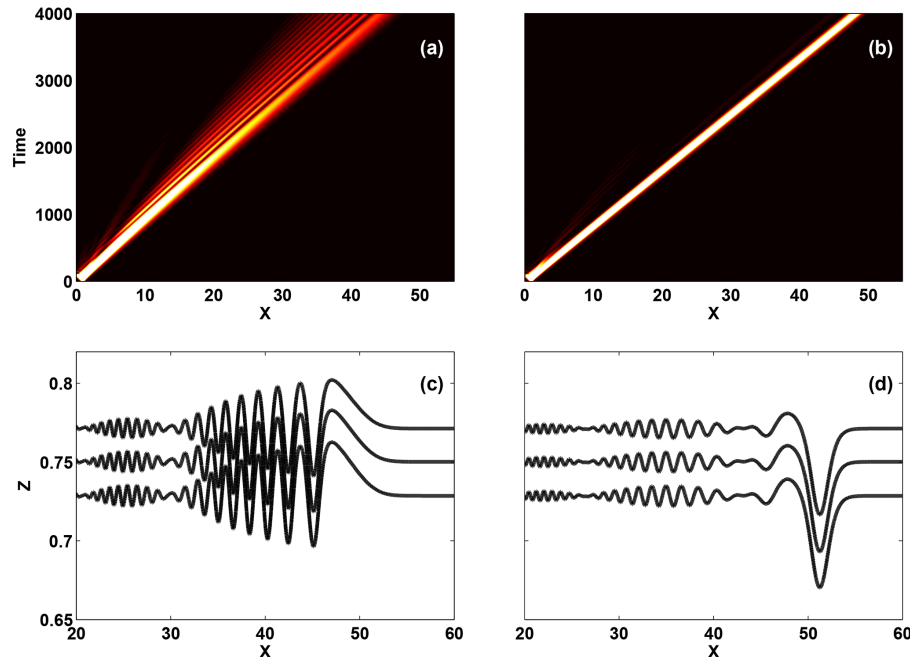
Figure 1. A space–time filled contour plot of vertically integrated kinetic energy and density iso-contours at $t = 450\,\text{s}$ (4275) showing the differences between the positive and negative polarity initial conditions with $w = \frac{1}{2}w_0$. **(a)** and **(c)** correspond to the positive polarity case while **(b)** and **(d)** to the negative case.

Discussion Paper | Discussion Paper | Discussion Paper | Discussion Paper | Discussion Paper

NPGD

doi:10.5194/npg-2015-73

Fully nonlinear stratified geostrophic adjustment problem

A. Coutino and M. Stastna
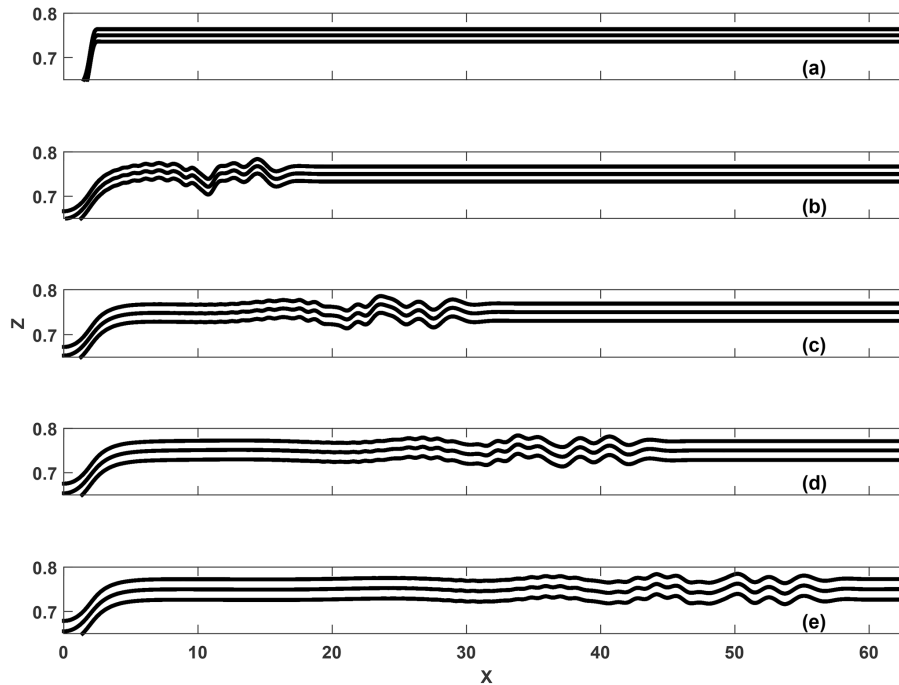
Figure 2. A line plot of density contours which show the time evolution of the waves generated **(a)** corresponds to $t = 0\,\text{s}$ (0), **(b)** to $t = 150\,\text{s}$ (15.75), **(c)** to $t = 300\,\text{s}$ (31.5), **(d)** to $t = 450\,\text{s}$ (47.25) and **(e)** to $t = 600\,\text{s}$ (42).

Discussion Paper | Discussion Paper | Discussion Paper | Discussion Paper | Discussion Paper

NPGD

doi:10.5194/npg-2015-73

Fully nonlinear stratified geostrophic adjustment problem

A. Coutino and M. Stastna
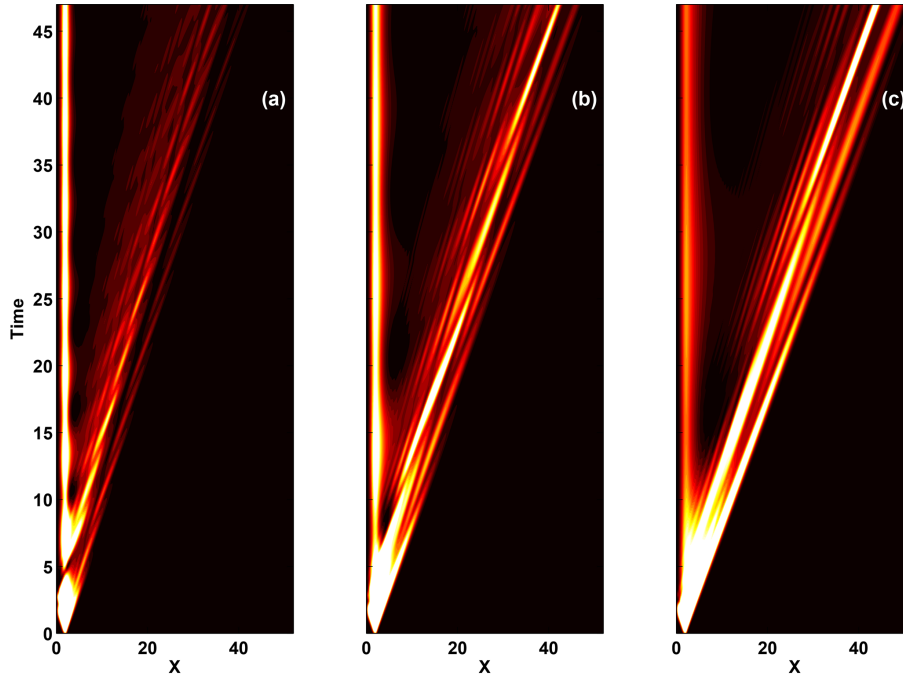
Figure 3. A space–time plot of the vertically integrated kinetic energy for different values of f. **(a)** corresponds to the $f = f_0$ case, **(b)** corresponds to the $f = \frac{1}{2}f_0$ case and **(c)** to the $f = \frac{1}{4}f_0$.

Discussion Paper | Discussion Paper | Discussion Paper | Discussion Paper | Discussion Paper

NPGD

doi:10.5194/npg-2015-73

Fully nonlinear stratified geostrophic adjustment problem

A. Coutino and M. Stastna
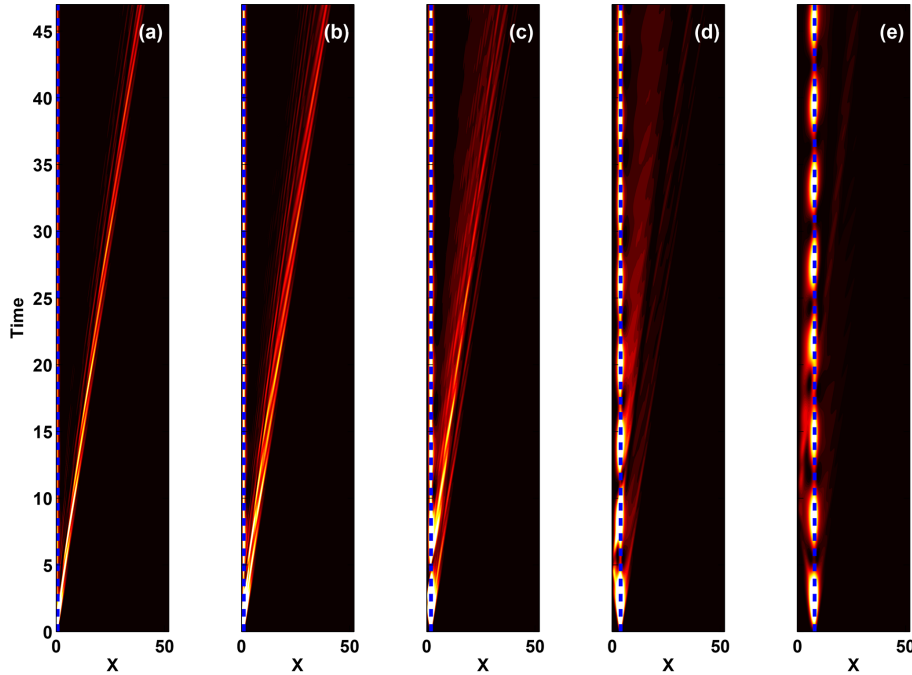
Figure 4. A space–time plot of kinetic energy for different values of w: **(a)** $w = \frac{1}{4}w_0$, **(b)** $w = \frac{1}{2}w_0$, **(c)** $w = w_0$, **(d)** $w = 2w_0$, and **(e)** $w = 4w_0$. The blue dashed line corresponds to the midpoint of the geostrophic state.

Discussion Paper | Discussion Paper | Discussion Paper | Discussion Paper

NPGD

doi:10.5194/npg-2015-73

Fully nonlinear stratified geostrophic adjustment problem

A. Coutino and M. Stastna
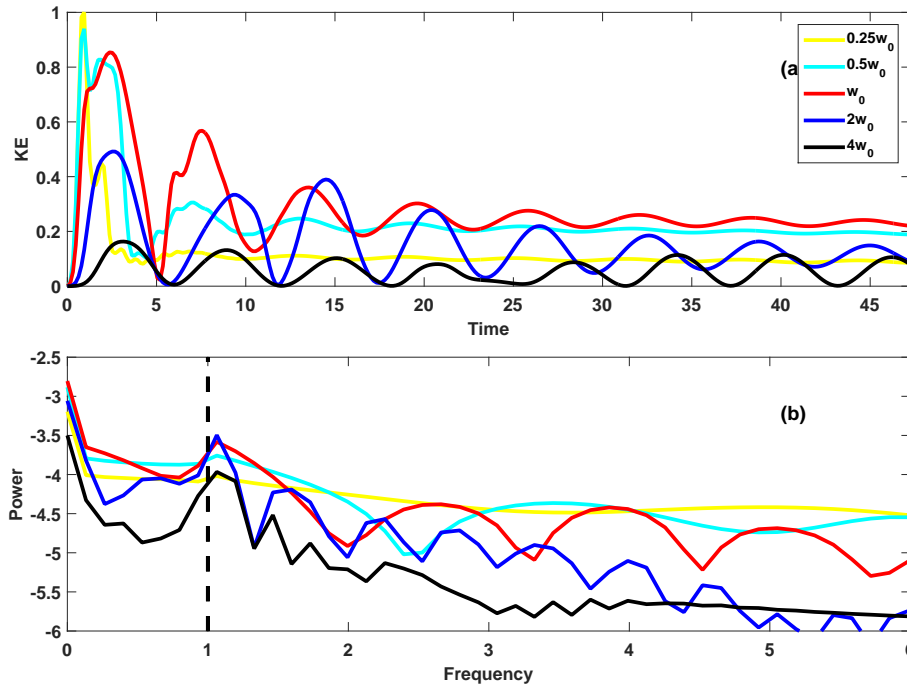
Figure 5. (a) shows a line plot of the vertically integrated kinetic energy found at the midpoint of the geostrophic state for different initial widths through time. **(b)** corresponds to the logarithm of the spectral power of the time series from **(a)**. The colours represent the different initial rotation rates and the dotted vertical line in **(b)** is the location of the inertial frequency.
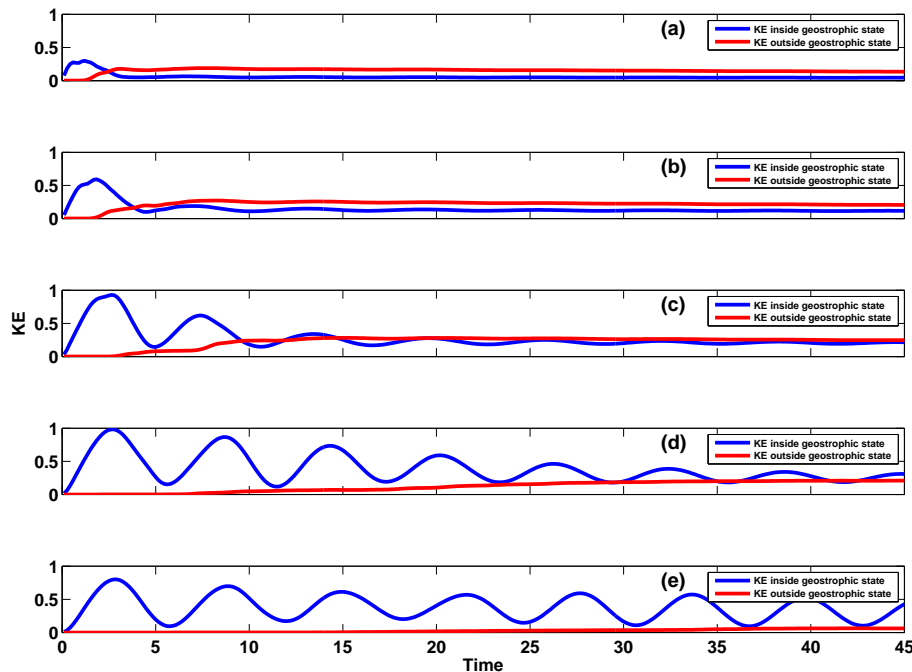
Figure 6. The total kinetic energy located inside (blue) and outside (red) of the geostrophic state. The different panels correspond to the different cases seen in Fig. 4: **(a)** to $w = \frac{1}{4}w_0$, **(b)** to $w = \frac{1}{2}w_0$, **(c)** to $w = w_0$, **(d)** to $w = 2w_0$, and **(e)** to $w = 4w_0$.

Discussion Paper | Discussion Paper | Discussion Paper | Discussion Paper | Discussion Paper

NPGD

doi:10.5194/npg-2015-73

Fully nonlinear stratified geostrophic adjustment problem

A. Coutino and M. Stastna

Discussion Paper | Discussion Paper | Discussion Paper | Discussion Paper | Discussion Paper

NPGD

doi:10.5194/npg-2015-73

Fully nonlinear stratified geostrophic adjustment problem

A. Coutino and M. Stastna
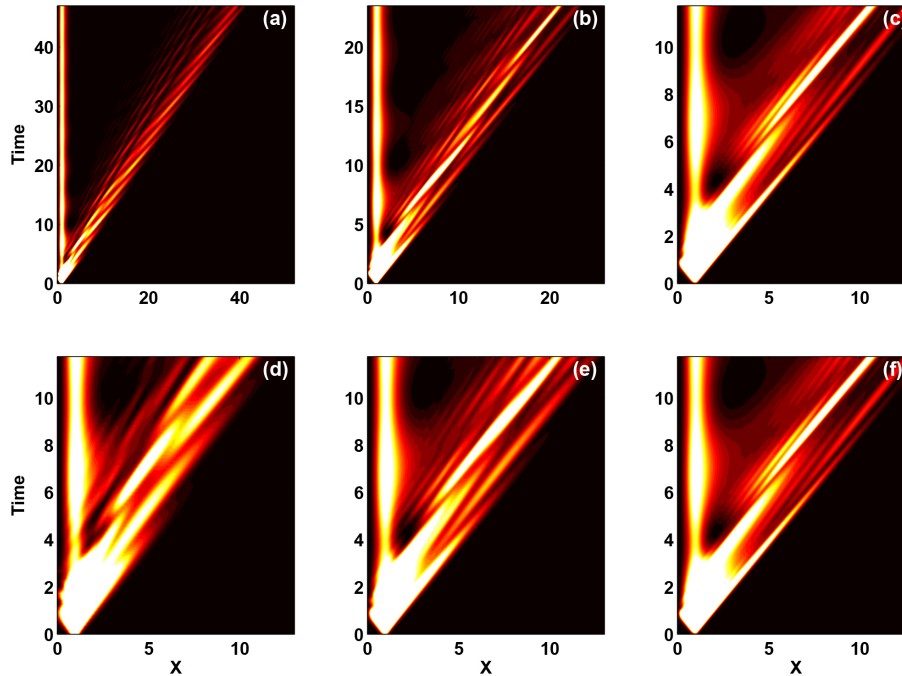
Figure 7. A space–time plot of kinetic energy. The different columns correspond to different f and w used to form a value of $Ro = 1$. **(a)** $f = f_0$ and $w = \frac{1}{2}w_0$, **(b)** $f = \frac{1}{2}f_0$ and $w = w_0$ and **(c)** $f = \frac{1}{4}f_0$ and $w = 2w_0$. The second row corresponds to the same case as the first columns but the aspect ration has been scaled by the rotation rate.

NPGD

doi:10.5194/npg-2015-73

Fully nonlinear stratified geostrophic adjustment problem

A. Coutino and M. Stastna
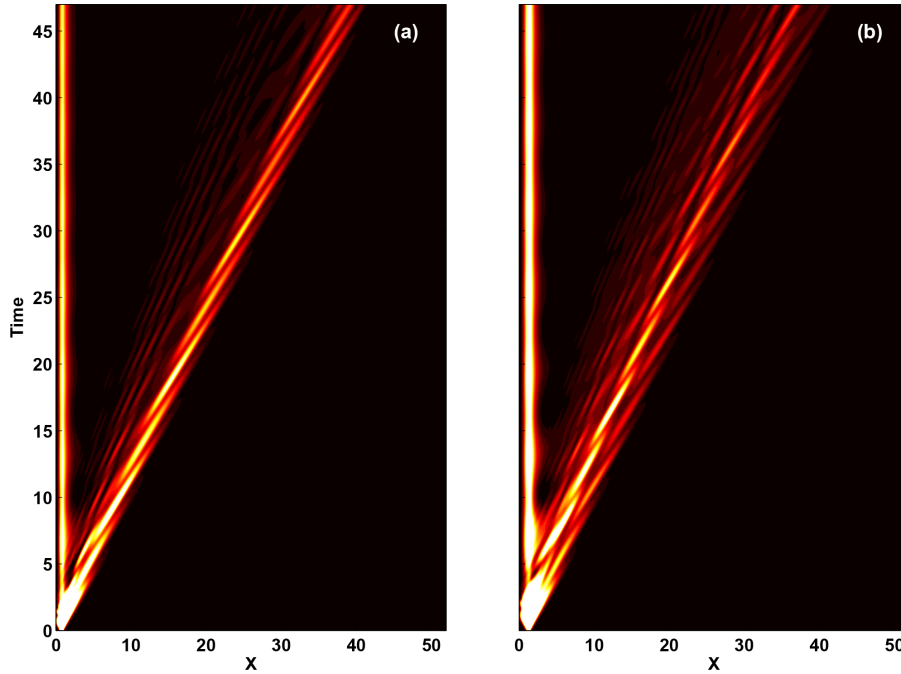
Figure 8. A space–time plot of kinetic energy for the near one Rossby number cases. **(a)** corresponds to the above $Ro = 1.25$ case, while **(b)** corresponds to the below $Ro = 0.75$ case.

Discussion Paper | Discussion Paper | Discussion Paper | Discussion Paper

NPGD

doi:10.5194/npg-2015-73

Fully nonlinear stratified geostrophic adjustment problem

A. Coutino and M. Stastna
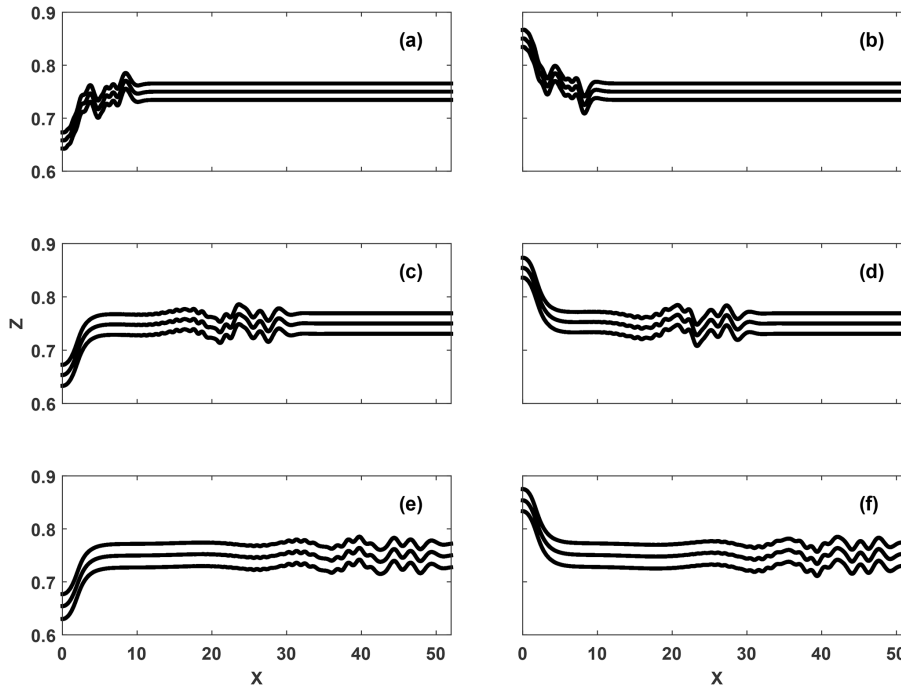
Figure 9. A sequence of snapshots of density iso-contours for the two different polarities of initial waves. **(a)** and **(b)** are at $t = 75\,\text{s}$ (5.25), **(c)** and **(d)** are at $t = 300\,\text{s}$ (21) and **(e)** and **(f)** are at $t = 525\,\text{s}$ (36.75).

NPGD

doi:10.5194/npg-2015-73

Fully nonlinear stratified geostrophic adjustment problem

A. Coutino and M. Stastna

Figure 10. A space–time plot of kinetic energy comparing positive and negative polarity initial conditions. **(a)** corresponds to an initial wave of depression, while **(b)** to a wave of elevation.
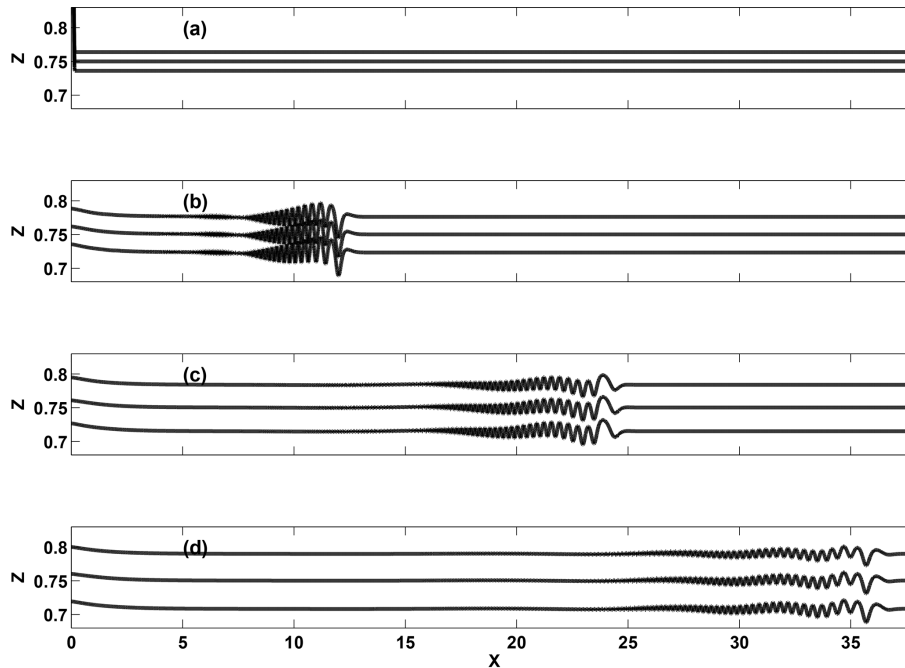
Figure 11. A long-time contour plot of the density field for the case where $f = \frac{1}{8}f_0$ and $w = \frac{1}{2}w_0$. **(a)** corresponds to $t = 0(0)$, **(b)** to $t = 900\,\text{s}$ (11.8), **(c)** to $t = 1800\,\text{s}$ (23.6) and **(d)** to $t = 2700\,\text{s}$ (35.4)

Discussion Paper | Discussion Paper | Discussion Paper | Discussion Paper

NPGD

doi:10.5194/npg-2015-73

Fully nonlinear stratified geostrophic adjustment problem

A. Coutino and M. Stastna

Discussion Paper | Discussion Paper | Discussion Paper | Discussion Paper

NPGD

doi:10.5194/npg-2015-73

Fully nonlinear stratified geostrophic adjustment problem

A. Coutino and M. Stastna
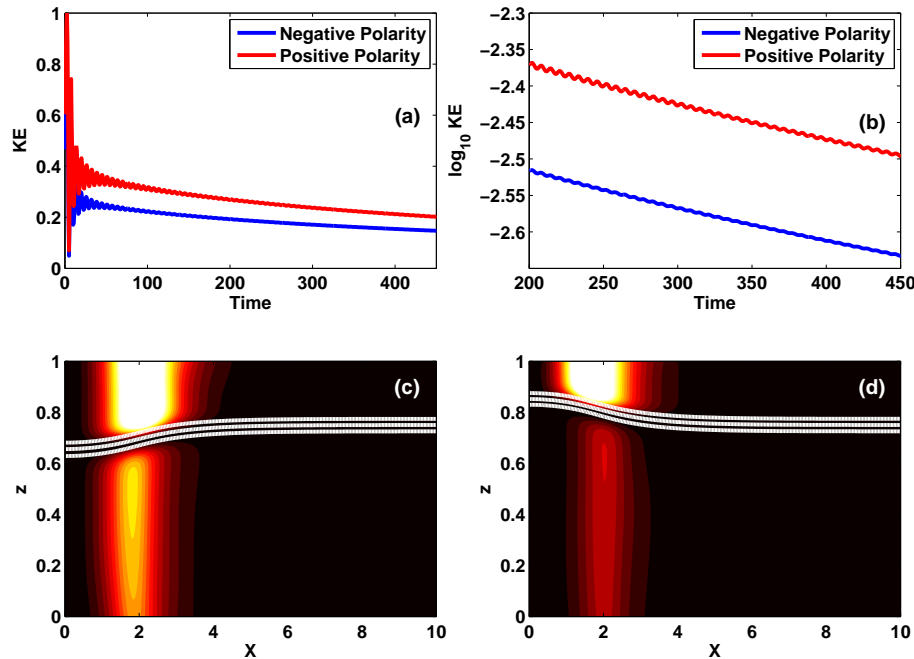
Figure 12. A series of different plots all highlighting features of the geostrophic state for positive and negative polarity cases. **(a)** presents the long-time time-series of vertically integrated kinetic energy in the geostrophic state. **(b)** shows the base ten logarithm of the geostrophic state kinetic energy after the packet has been ejected. (**c** and **d**) show the total kinetic energy in the geostrophic state, along with contours of constant density, for a negative and positive initial polarity respectively.

Discussion Paper | Discussion Paper | Discussion Paper | Discussion Paper

NPGD

doi:10.5194/npg-2015-73

Fully nonlinear stratified geostrophic adjustment problem

A. Coutino and M. Stastna
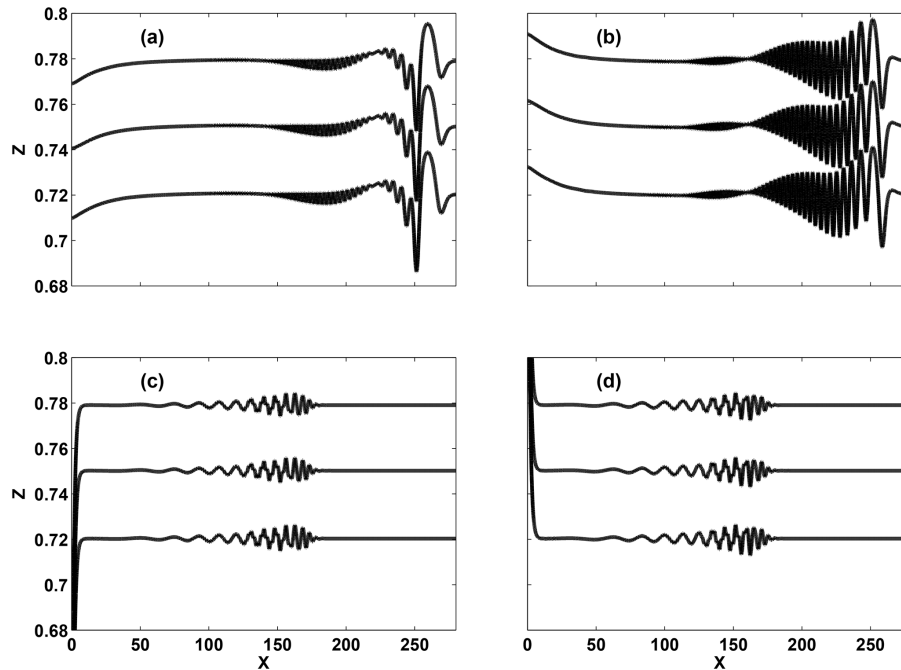
Figure 13. A series of comparisons of the density field across two different rotation rates, $f = 2f_0$ and $f = \frac{1}{8}f_0$ and the two polarities. **(a)** corresponds to $f = \frac{1}{8}f_0$ and negative polarity, **(b)** to $f = \frac{1}{8}f_0$ and positive polarity, **(c)** to $f = 2f_0$ and negative polarity and **(d)** to $f = 2f_0$ and positive polarity.
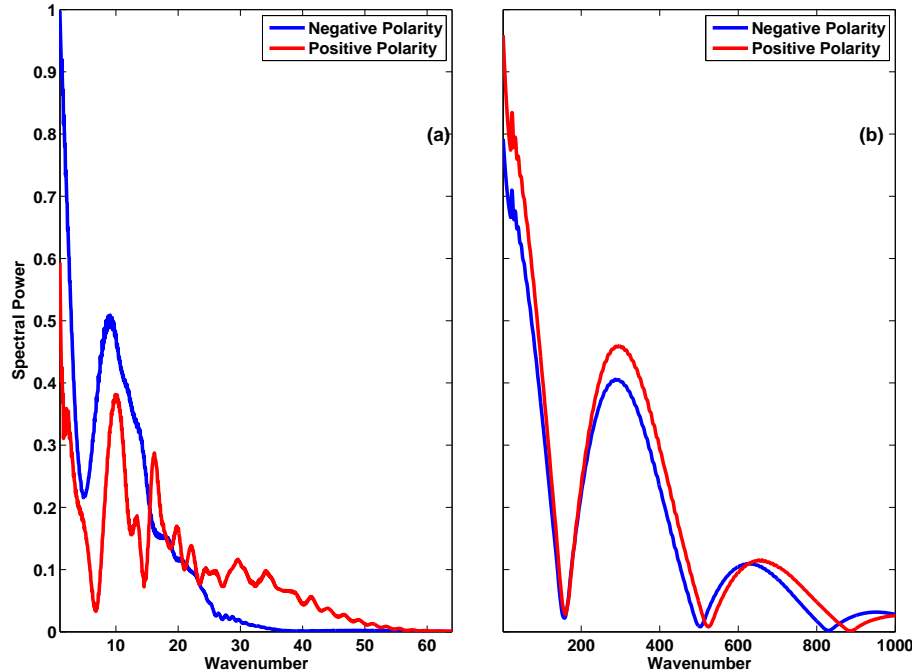
Figure 14. Comparison of the scaled, filtered spectra for different polarities, where **(a)** corresponds to a "low" $f = \frac{1}{8}f_0$ and **(b)** corresponds to a "high" $f = 2f_0$. This figure is taken at 1200 s (15.8 for **(a)** and 252 for **(b)**) and the initial width is $w = \frac{1}{2}w_0$. The spectra has been scaled by the maximum value for each case and the wave-number has been scaled by $\frac{2\pi}{Ro_r}$.

Discussion Paper | Discussion Paper | Discussion Paper | Discussion Paper

NPGD

doi:10.5194/npg-2015-73

Fully nonlinear stratified geostrophic adjustment problem

A. Coutino and M. Stastna

Title Page

Abstract · Introduction

Conclusions · References

Tables · Figures

|◄ · ►|

◄ · ►

Back · Close
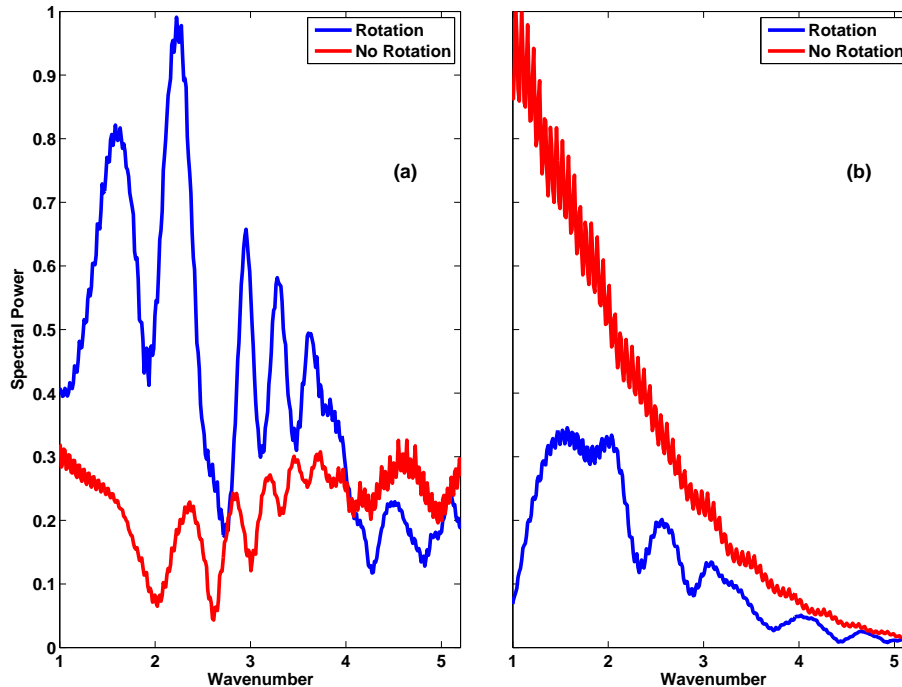
Figure 15. Comparison of the scaled, filtered spectra for no rotation and $f = \frac{1}{8}f_0$, where **(a)** corresponds to an initial wave of elevation and **(b)** corresponds to an initial wave of depression. This figure is taken at 2250 s (29.5 in the rotating case and 236.8 in the non rotating case) and the initial width is $w = \frac{1}{2}w_0$. The spectra have been scaled by the maximum value between the cases and the wave-number has been scaled by $\frac{2\pi}{Ro_r}$.

Discussion Paper | Discussion Paper | Discussion Paper | Discussion Paper | Discussion Paper |

NPGD

doi:10.5194/npg-2015-73

Fully nonlinear stratified geostrophic adjustment problem

A. Coutino and M. Stastna